Journal of Materials Science and Engineering with Advanced Technology
Volume 3, Number 1, 2011, Pages 1-27

FRETTING FATIGUE BEHAVIOUR OF IN100 AT ROOM TEMPERATURE

S. MALL[1], E. MADHI[1] and H.-K. KIM[1,2]

[1]Department of Aeronautics and Astronautics
Air Force Institute of Technology
Wright-Patterson AFB, OH 45433
U.S.A.
e-mail: shankar.mall@afit.edu

[2]Technical Development Center
Agency for Defense Development
P.O. 35-5, Yuseong
Taejeon, 305-600
Korea

Abstract

Fretting fatigue behaviour of a nickel based alloy, IN100, was investigated at room temperature. Fretting fatigue tests were conducted at various stress levels by using two cylindrical pad geometries. Fretting fatigue crack initiation location and orientation angle were documented. Fretting reduced the strength/life in comparison to those in the plain fatigue; however, this reduction was relatively less than that in titanium alloy, Ti-6Al-4V. Both IN100 and Ti-6Al-4V are used in gas turbine engines. Increase in cylindrical pad radius had relatively less detrimental effect on the fretting fatigue life/strength of IN100 relative to those of titanium alloy, Ti-6Al-4V. The primary fretting fatigue crack initiated near the trailing edge on the contact surface, and at an orientation of 45° with a variation of ±10°. Finite element analysis was also conducted to obtain the stress state in the contact region, which was then used to compute a critical plane based

Keywords and phrases: fretting, fatigue, IN100, critical plane parameter, contact mechanics.

Received July 21, 2010

parameter, modified shear stress range parameter, involving both normal and shear stresses on the critical plane. This parameter was found to be capable of predicting crack location, crack initiation angle and correlating the fretting fatigue lives of two contact geometries and plain fatigue lives on a single curve.

1. Introduction

Fretting occurs at the interface between mating bodies that are undergoing an oscillatory motion of small amplitude and are subjected to clamping force. This generally causes a considerable reduction in the life of structural/machine components compared to the plain fatigue, i.e., conventional fatigue without fretting. This phenomenon is known as the *fretting fatigue*. Under fretting fatigue, tensile and shear stresses are increased in the contact region leading to surface or subsurface damage, which act as the stress concentration site promoting faster crack nucleation/initiation/growth. Fretting induced damage occurs in several structural/machine components, e.g., riveted/bolted joints, metallic cables, coil wedges, snap fit areas, and other clamped members. Fretting fatigue is also prevalent in the dovetail joints, i.e., at the interface between the engine disk slot and blade attachments in the gas turbine engines. Not only fretting fatigue causes an increase in maintenance costs, but also results in a significant reduction in aircraft and engine component's service life. As a result, fretting fatigue is of great interest to the aerospace engine community.

Previous fretting fatigue studies have involved several aspects, one of which is how fatigue life/strength of a material is affected by the fretting action. In this arena, the effects of various factors/phenomena, such as magnitude of applied cyclic stress, contact pressure, contact geometry, environment, surface condition, loading condition, etc. have been investigated [1, 5, 7]. Further, these studies have been conducted with several important engineering materials: carbon steels (SAE 1045, SA-516, J1S S35C), high strength steels (AISI 4340, SNCM 439), stainless steels (SA-240-410S, PH 13-8 Mo, 15Cr 11Mo V), Ni-Mo-V steel, aluminum alloys (2024, 7075, 8090), titanium alloys (Ti-6Al-4V, Ti-6242) etc. [1, 5, 7]. On the other hand, limited numbers of studies are reported on the fretting fatigue behaviour of nickel based alloys even though they

are widely utilized in both land-based and aero-gas turbine industries. Attia [2] investigated the fretting fatigue of two nickel-based alloys, Inconel 600 and Inconel 800 when in contact with carbon steel and 410S stainless steel in the steam environment at 265°C. The nickel-based alloys have been also used as one of the contacting materials (i.e., as fretting pad) to investigate the fretting fatigue behaviour of titanium alloy [3, 9, 10, 14]. Murthy et al. [15, 16] investigated the fretting fatigue behaviour of single crystal nickel alloy in contact with polycrystalline nickel alloy at 610°C. Kwon et al. [8] investigated the fretting and plain fatigue behaviours of Inconel 690 at the room temperature. Mall et al. [13] characterized the fretting fatigue behaviour of shot-peened titanium alloy, Ti-6Al-4V and shot-peened nickel based alloy, IN100 at the room temperature.

The objective of this study was to characterize fretting fatigue behaviour of IN100 at room temperature under ambient laboratory condition. This material is of a great interest to both land-based and aero-gas turbine industries, where several applications commonly experience fretting fatigue. In particular, fretting fatigue tests were conducted with the cylinder-on-flat fretting configuration with two radii, 50.8mm and 304.8mm. In addition, plain fatigue (i.e., conventional fatigue without fretting) tests were conducted to evaluate the effect of fretting on fatigue life. The tests were conducted at different axial stress levels that comprised both the low cycle and high cycle fatigue regimes. Further, finite element analysis was conducted to determine the stress, strain, and displacement fields in the contact region. The finite element results were then used to evaluate a critical plane based fatigue parameter to analyze the fretting fatigue behaviour of IN100.

2. Experiments

2.1. Materials

The test material of this study was a powder processed nickel-based super alloy, P/M IN-100. It was obtained in the form of an extruded bar, which was produced through the following manufacturing processes; gas atomization, canning and degassing of alloy powder, hot compaction, pre-

heating at 1070K, and hot extrusion with a reduction ratio of 11. The nominal composition of the material is Ni-5.0, Al-3.2, Mo-4.3, Ti-0.8, V-12.4, Cr-18.5, Co-0.07, Zr-0.02, B-0.07 (wt%). Its elastic modulus, yield strength, ultimate strength, and Poisson's ratio are 196GPa, 1150MPa, 1520MPa, and 0.28, respectively. The microstructure of the material is shown in Figure 1. Figure 1(a) shows that a homogeneous structure of fine γ' particles dispersed in a γ matrix with volume fractions of about 60%, which is produced by hot extrusion even though there is some local directional array of γ' particles, which represents microstructural features of solidified powders. At higher magnification, shown in Figure 1(b), it can be seen that two different size of γ' phase are embedded in the γ matrix, which are of $1 \sim 2\mu m$ primary γ' phase mainly formed during solidification of powders and about $0.25\mu m$ secondary γ' phase precipitated and grown during cooling stages of solidification and/or extrusion processes, respectively. Figure 1(b) also shows that the size of γ grain is comparable with that of a large primary γ' phase. The average grain size of the γ matrix was about $4\mu m$.

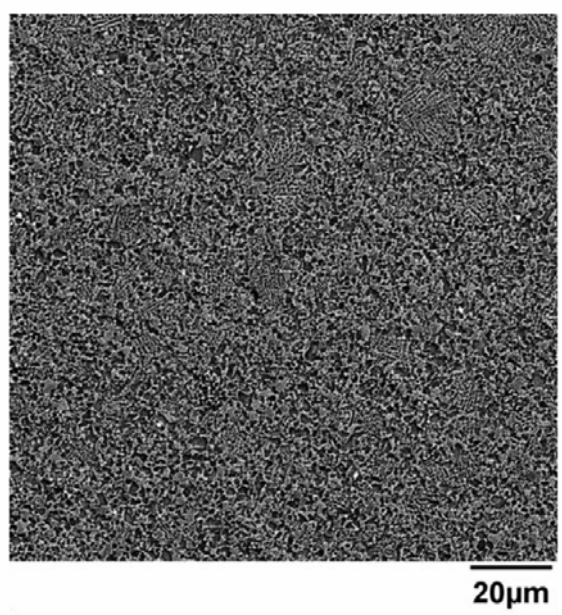

(a)

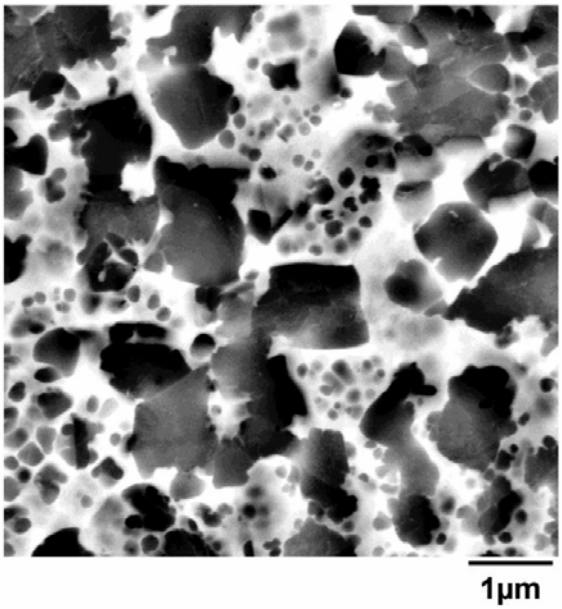

(b)

Figure 1. Microstructural details of IN100 of this study.

2.2. Specimen details

Test specimen was of the dog-bone shape with thickness equal to 3.8mm, width equal to 6.4mm, and total length equal to 127mm. It is shown schematically in Figure 2. The pads had cylindrical ends, with either 50.8mm or 304.8mm radius. The thickness and the width of both pad types were both 9.5mm. Both pads and specimens were from IN100. Both were machined by the electrical wire discharge method, ground and finally, hand polished to a finish having surface roughness, R_a = 0.2μm.

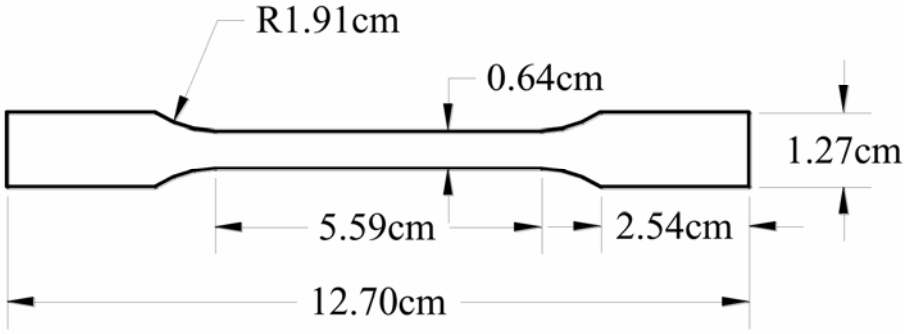

Figure 2. Fretting fatigue specimen.

2.3. Test details

A servo-hydraulic fatigue test machine equipped with a fretting test set-up was used, Figure 3.

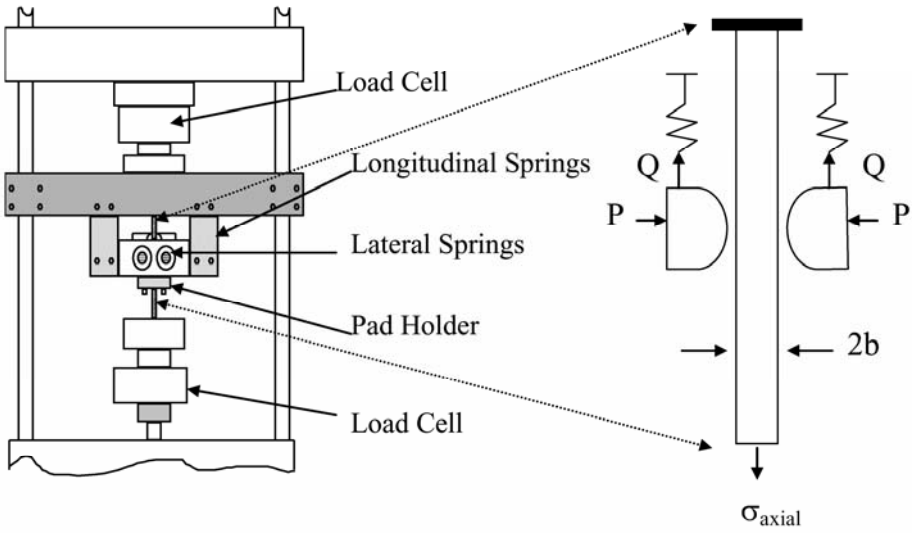

Figure 3. Fretting fatigue test set-up.

The details of fretting test set-up and fretting test procedure are reported in previous studies [11, 12, 17]. Several tests were conducted under tension-tension fatigue condition at different stress levels, σ ranging from 600MPa to 1100MPa, with a constant stress ratio of 0.1. The cyclic axial load on the specimen was applied in the length direction through the servo-hydraulic test machine with constant amplitude at frequency of 10Hz. A pair of pads was pressed on both width faces of the specimen through the fretting fixture. The normal contact load, P on the pad was 4000N. The tangential load, Q was generated by pads. The tangential force, Q was determined from the measured loads on the each side of the specimen [11, 12, 17]. The cyclic axial loads and tangential loads were recorded throughout the test. The tangential force, Q increased initially in a fretting test, but it stabilized between 100 to 500 cycles in a test. A typical variation of tangential force, Q with cycling is shown in Figure 4.

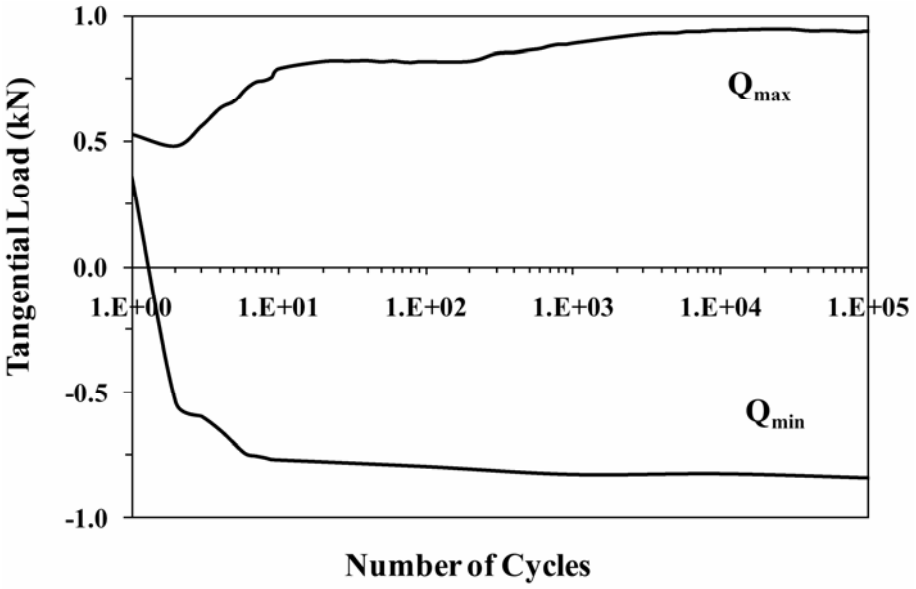

Figure 4. Variation of tangential load during a fretting fatigue test.

The experimentally stabilized value of tangential force and contact load (Q/P) ratio ranged from 0.30 to 0.4 in this study. It ranged from 0.1 to 0.2 at the beginning of test and it increased with cycling during first 100 to 500. The ratio of tangential force and contact load (Q/P) is also referred to as dynamic coefficient of friction, which is different than kinetic coefficient of friction. The latter is the friction under gross sliding condition [20]. On the other hand, the ratio of incipient load (Q_{slip}) at which initial slip occurs to the applied normal contact load (P) is the static coefficient of friction. The static coefficient of friction was determined experimentally before the fretting tests as per the procedure described in a previous study [6]. This was equal to 0.45 ± 0.02. For this measurement, the specimen was gripped in the lower end in the test machine (Figure 3), and normal contact load of 4000N was applied on the pads. Then, the axial load was increased slowly till there was initiation of slip between specimen and pads at which instant incipient slip load was recorded. All tests involved the partial slip condition that was verified from the hysteresis loops between axial load and tangential force. These were of the slender elliptical shape representative of the partial slip condition as shown typically in Figure 5.

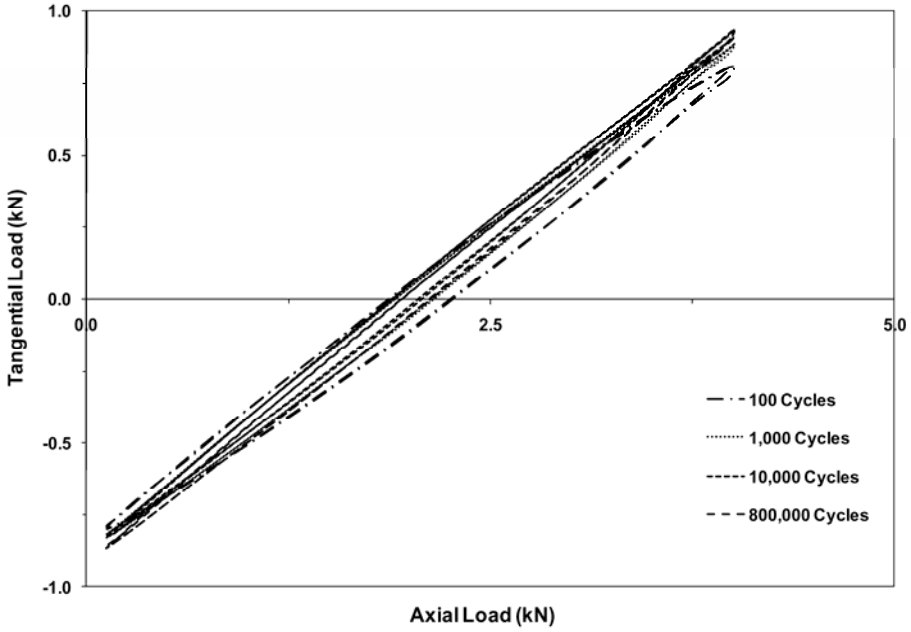

Figure 5. Hysteresis loops during a fretting fatigue test.

2.4. Damage details

A typical fretting scar on the specimen fretted with 50.8mm radius pad is shown in Figure 6. The fretting fatigue scar had a stick zone in the center area with darker thin region on the edges denoting partial slip zones at the leading and the trailing edges of the contact area. The average experimental contact width, $2a$, was about 1.1mm and 2.7mm for pad radii of 50.8mm and 304.8mm, respectively. The corresponding analytical values were 1.2mm and 2.9mm, respectively [4], resulting in a difference of about 10% from the experimental values. In all tests of this study, crack initiation location was near the trailing edge (slip/no-slip boundary on the contact surface), i.e., at a location of $x/a \sim 1.0$, as shown in Figure 6, where x is the distance along the crack surface from the center of the contact width.

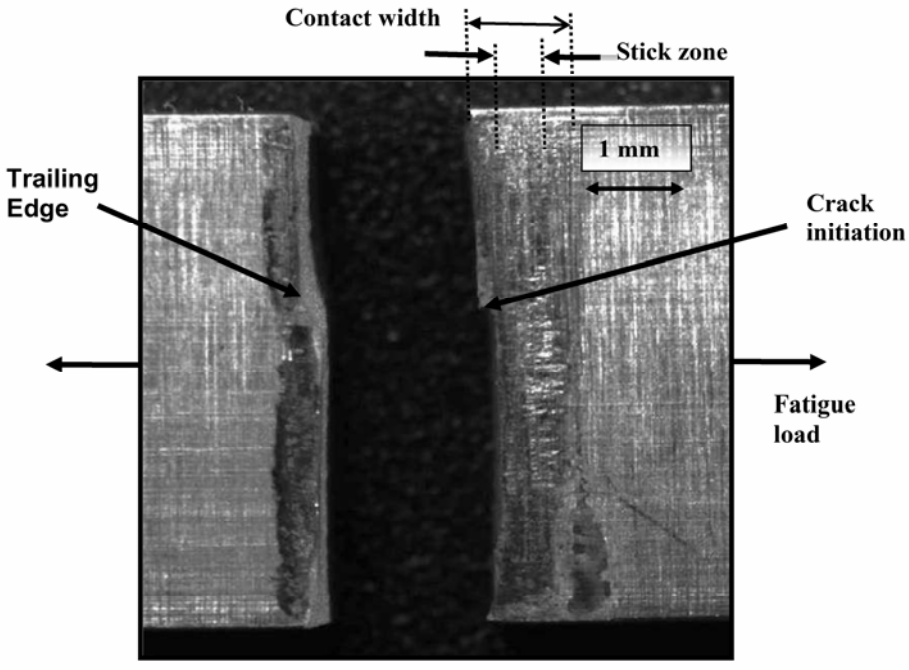

Figure 6. Typical fretting scar on specimen fractured from fretting fatigue.

Once the crack initiated, the applied stress became asymmetric. Thereafter, the crack growth was not coplanar and hence not perpendicular to the applied load direction. This caused crack to grow within the contact width later away from the initiation location as shown in Figure 7.

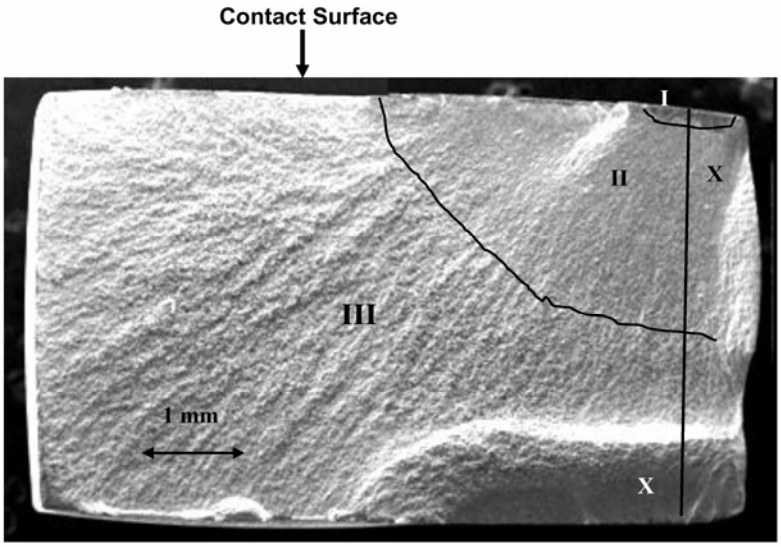

(a)

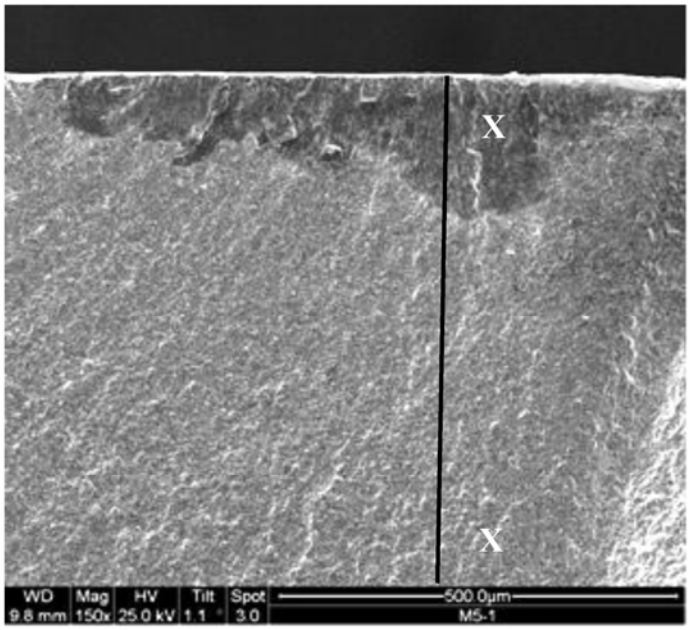

(b)

Figure 7. Fracture surface; (a) complete view with three regions, (b) close-up view of region I.

Crack initiation was on the contact surface, which is evident also on the fracture surface shown in Figure 7. The fracture surface showed three distinct regions; fatigue crack initiation (region I), propagation (region II), and tensile overload (region III). The magnified views of all these three regions are shown in Figure 8. As shown in Figure 8(a), no distinct cleavage facets representing crystalline cracking were observed, but very small facets surrounding hollows are evident suggesting that the coarse primary γ' particles had been pulled out. It indicates that cracks were developed by cutting through γ grains and propagated by passing around the coarse primary γ' particles. Figure 8(b) shows that the fatigue crack propagation took place primarily in the trans-granular mode. Figure 8(c) shows that fracture surfaces mainly consisted of ductile dimples generated from coarse γ' particles and also γ grain boundaries.

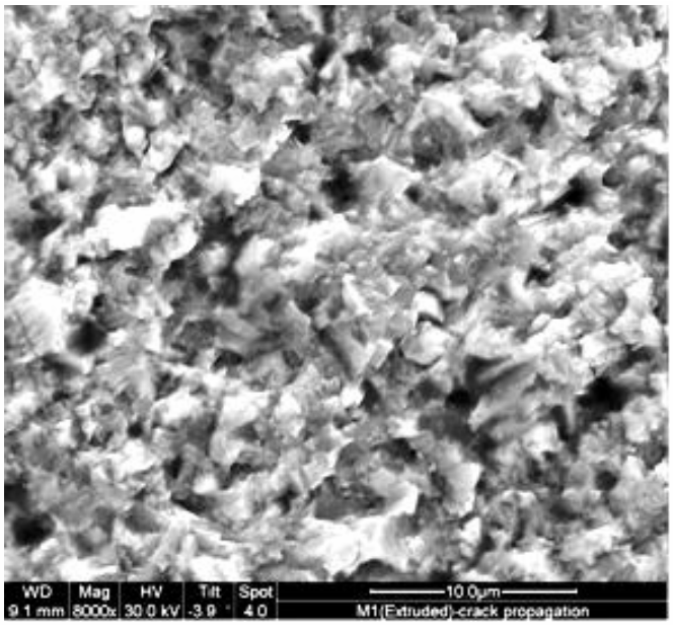

(a)

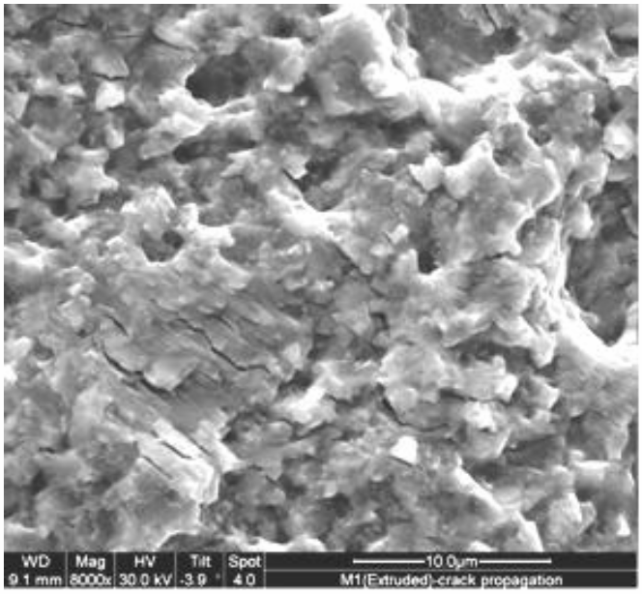

(b)

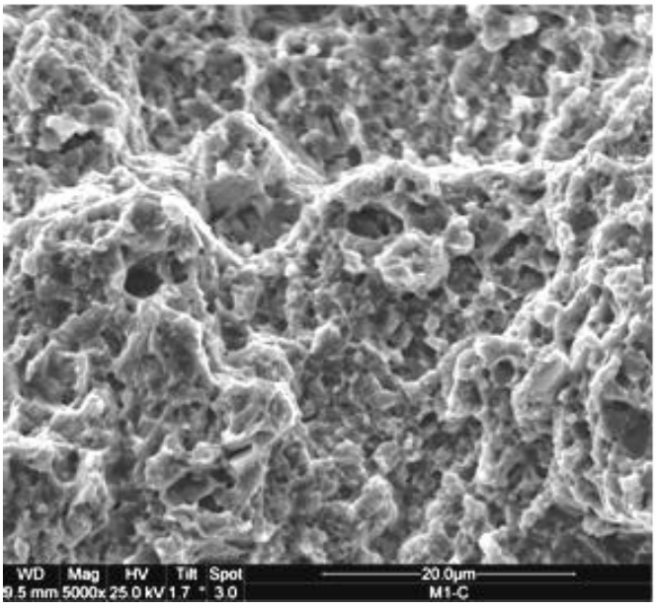

(c)

Figure 8. Microstructural details of fracture surface; (a) region I, (b) region II, and (c) region III.

Several specimens were then sectioned along the longitudinal direction of the specimen and perpendicular to the fracture surface, as indicated by line XX in Figure 7, then mounted in the epoxy, ground and polished near the crack initiation location. Figure 9 shows a representative micrograph showing the orientation of the primary crack, which caused the failure of specimen. It can be seen in the figure that the orientation of the primary crack near the initiation location on the contact surface was about 43° from a perpendicular to the applied load direction. Overall, orientations of the initiated crack at the contact surface were ±45° with 10° variation. The positive and negative orientations of angle (θ) are shown in Figure 9. Further, the orientation of these cracks changed to the 90°, i.e., perpendicular to the applied load direction at about 50 to 150μm from the contact surface. Similar damage characteristics were observed in Ti-6Al-4V [11, 12, 17].

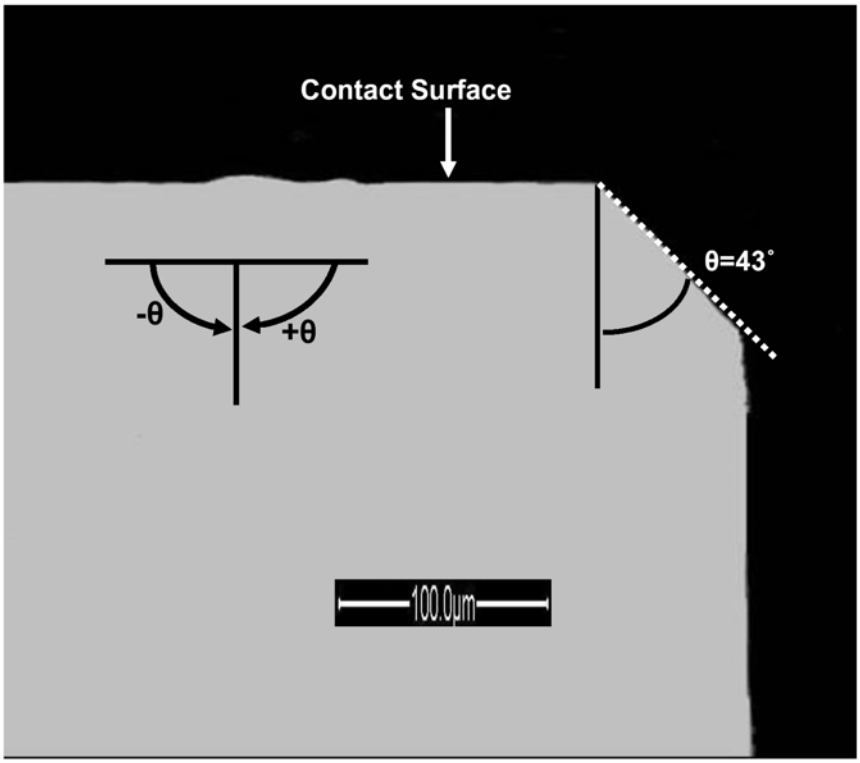

Figure 9. Fretting crack initiation orientation at contact surface.

3. Analysis

Finite element method, using the linear elastic formulation, was used to determine stress, strain, and displacement fields. The finite element technique was necessary because the half-space assumption was not satisfied due to the specimen's finite thickness, while the analytical solutions are for the semi-infinite domain [4]. The finite element model is shown in Figure 10, which shows one-half of the test configurations due to symmetry. Along with the "master-slave", interfacial algorithm developed for contact modelling in a commercially available finite element code, ABAQUS, the four-node plane elements were utilized. A small-sliding contact formulation was used, where parameter was set equal to 4×10^{-8} to adjust the initial positions of the contacting surfaces. These adjustments were made at the start of the analysis so that they did not create any prestrain. Friction between contacting surfaces used Lagrange multiplier formulation. All specimens were analyzed by using the measured loads, i.e., measured axial, contact, and tangential forces. These loads were applied to the model in the three steps during the analysis. In the first step, the normal load, P was applied to establish contact between pad and specimen. In the second and third steps, either the maximum bulk stress, $\sigma_{\text{axial, max}}$, and corresponding $Q_{\max}$ or the minimum bulk stress, $\sigma_{\text{axial, min}}$, and corresponding $Q_{\min}$ were applied, respectively.

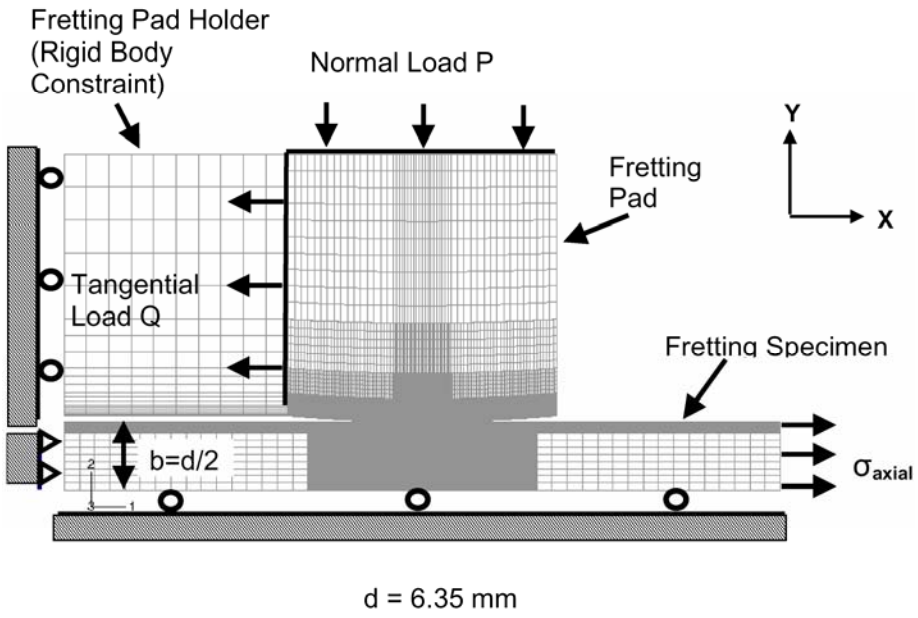

Figure 10. Finite element model.

The finite element mesh was refined in the contact region, until a suitable agreement was obtained between the finite element results and the analytical solution, which was less than 2%. Since the analytical solution is for the semi-infinite domain, the specimen width b was increased to 50mm in the convergence analysis only. An acceptable element size was determined to be $2\mu m \times 2\mu m$ in the refined contact zone from the convergence study. This procedure has been discussed in details in previous studies [11, 12, 17, 18], where mesh refinement was carried out until the computed stresses in the contact region were within 2% of those from the analytical solution.

Figure 11 illustrates the effect of the pad radius on the contact stresses, i.e., axial, shear, and transverse stress distribution when the specimen was subjected to the applied stress of 650MPa, tangential load of 600N, and contact load of 4000N. These stress distributions are shown along the contact surface as a function of x/a, where x is the distance from the center of contact zone and a is the half-contact width. The

stresses in Figure 11 are normalized with the applied axial stress of 650MPa. The maximum longitudinal normal stress, σ_{xx} is approximately 25% larger with the 50.8mm pad than that with the 304.8mm pad, both occurring near the trailing edge, $x/a = 1$ (Figure 11(a)). It is also interesting to note that the 50.8mm pad configuration generates the compressive longitudinal normal stress (σ_{xx}) near the center of contact area, while minimum stress for 304.8mm pad configuration is of the tensile nature in the center region of the contact area. For the 50.8mm pad configuration, the maximum shear stress (σ_{xy}) occurs near the center of contact, while its corresponding location for 304.8mm pad is at $x/a = 0.4$, Figure 11(b). Further, the maximum shear stress is approximately 2.5 times larger with the 50.8mm pad than that with the 304.8mm pad. The transverse normal stress (σ_{yy}) for both pad radii shows exactly the same overall symmetrical distribution. However, the maximum, Hertzian peak pressure (σ_{yy}) is approximately 2.3 times larger for the 50.8mm pad than that with the 304.8mm pad, Figure 11(c).

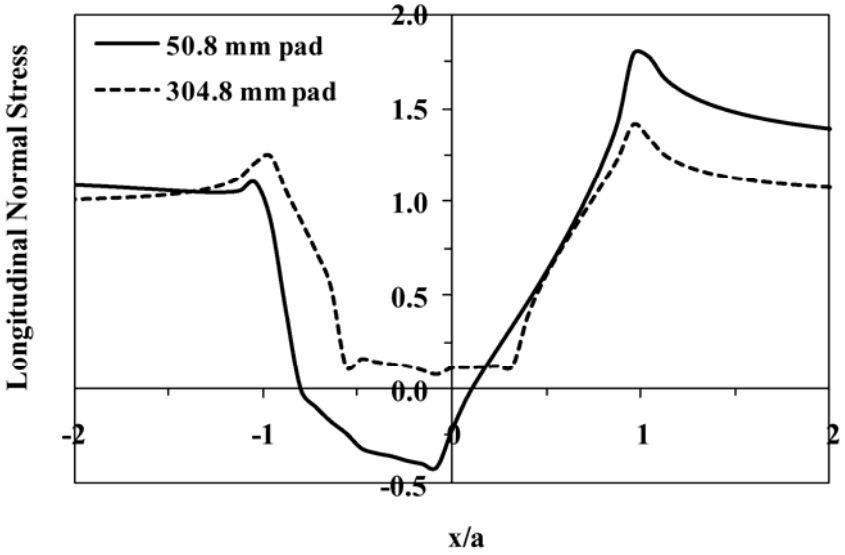

(a)

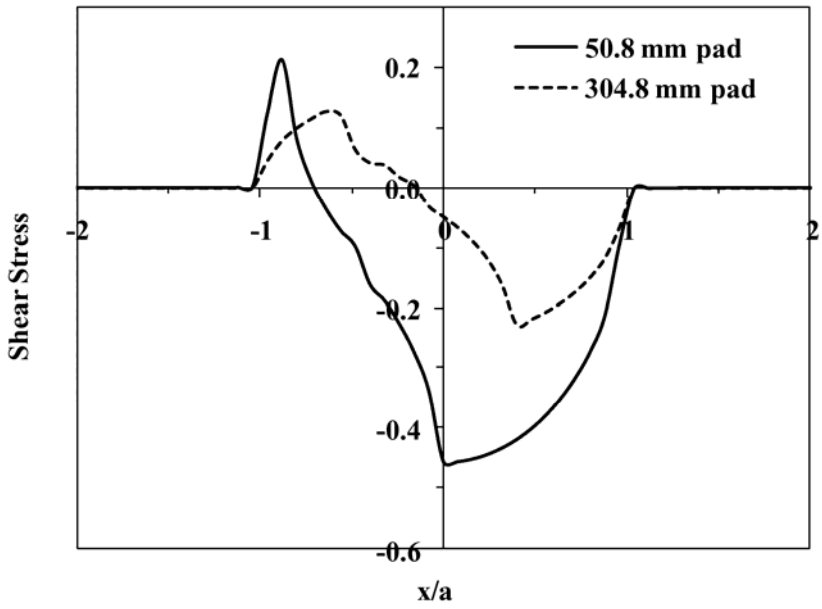

(b)

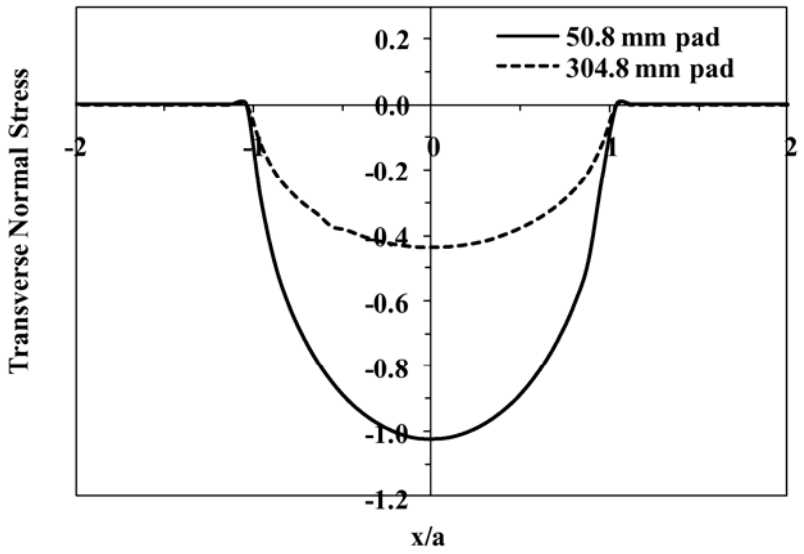

(c)

Figure 11. Contact stress state for two pad geometries; (a) longitudinal normal stress (σ_{xx}), (b) shear stress (σ_{xy}), and (c) transverse normal stress (σ_{yy}).

4. Results and Discussion

4.1. Fatigue life

Figure 12 shows the applied stress range (σ_{max} - σ_{min}) to the specimen versus fatigue life relationships of IN100, when fretted with 50.8mm radius and 304.8mm radii pads as well as the corresponding plain fatigue relationship. Figure 12 shows the typical characteristics of fretting fatigue life as commonly seen in many materials. There is a decrease in the fatigue strength of IN100 in the presence of fretting. In many metallic materials, the magnitude of this reduction due to the introduction of fretting has been reported in the range of 30 ~ 60% relative to plain fatigue [1, 5, 7]. So in essence, the fretting fatigue behaviour of IN100 does follow the same general trend of degradation relative to the plain fatigue. Since two different pad radii, 50.8mm and 304.8mm, were used in this study, the present study provided the effects from different pad radii, i.e., contact geometry, on the fretting fatigue behaviour of IN100. Figure 12 also illustrates this effect. It is interesting to note that changing the cylindrical pad radius from a higher curvature value (50.8mm) to nearly flat pad (304.8mm) had little effect on the fretting fatigue life. The fretting fatigue curves for the two pad configurations are certainly distinguishable, as can be seen from the two corresponding curves fitted to the data, however, they are not too far apart as is in the case of titanium alloy, Ti-6Al-4V [17].

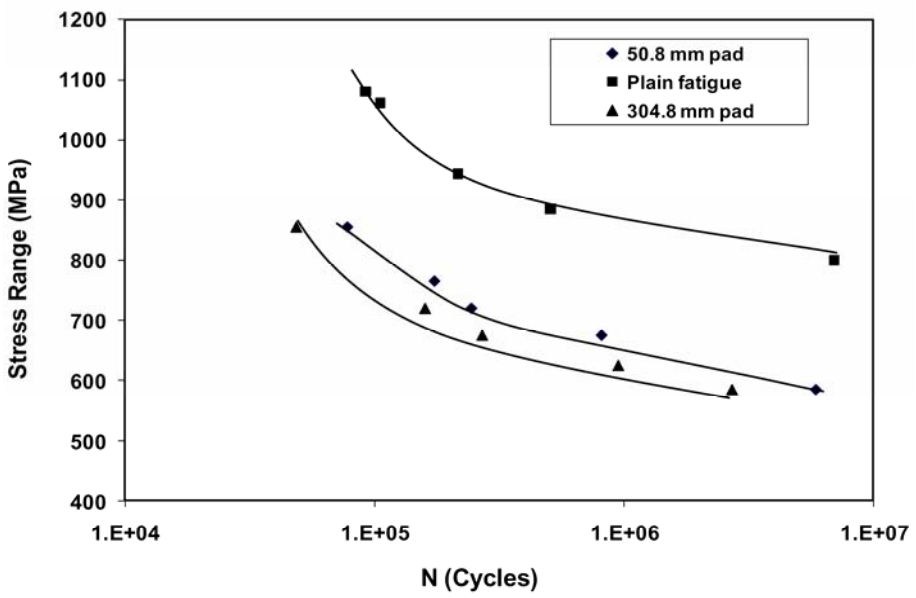

Figure 12. Fretting and plain fatigue life diagrams for IN100.

Ti-6Al-4V is another commonly used material in the land-based and aero-gas turbine industries. Figure 13 compares the fretting fatigue behaviour of these two materials, i.e., IN100 and Ti-6Al-4V. This figure shows the applied stress versus fretting fatigue life relationships for two contact geometries (50.8mm and 304.8mm radii cylindrical pads) for both IN100 and Ti-6Al-4V on the basis of effective applied stress on the specimen, which is defined as [19]:

$$\sigma_{\text{eff}} = \sigma_{\max}(1 - R)^m, \tag{1}$$

where R is the stress ratio and m is a fitting constant, which was equal to 0.45 [17]. This approach was taken since fretting fatigue tests for Ti-6Al-4V were conducted at different stress ratios [19]. Figure 13 also shows that IN100 has relatively less reduction in fatigue strength/life in the presence of fretting in comparison to Ti-6Al-4V, and the reduction depends upon the contact geometry.

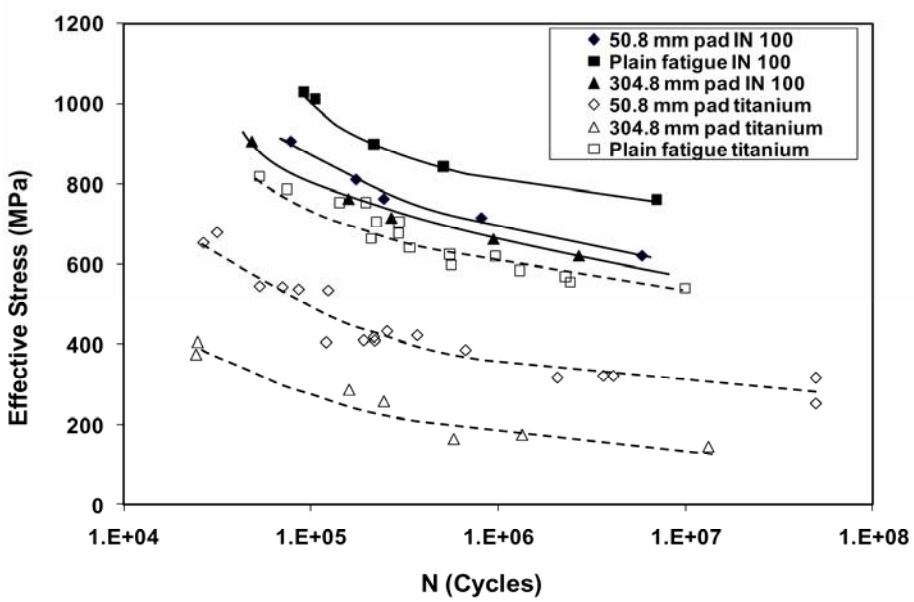

Figure 13. Comparison of fretting and plain fatigue life lives for IN100 and Ti-6Al-4V.

The increase in cylindrical pad radius had relatively less detrimental effect on the fretting fatigue life/strength of IN100 relative to those of titanium alloy, Ti-6Al-4V. This is shown also in an alternate way in Figure 14, where fretting strength at a given fatigue life is normalized by the corresponding plain fatigue strength for both materials and contact geometries. This figure again shows the features, which were stated earlier that IN100 is relatively more resistant to fretting than Ti-6Al-4V, and relatively flatter contact geometry (i.e., larger contact area) causes more degradation during fretting. These characteristics are of great relevance during their practical applications.

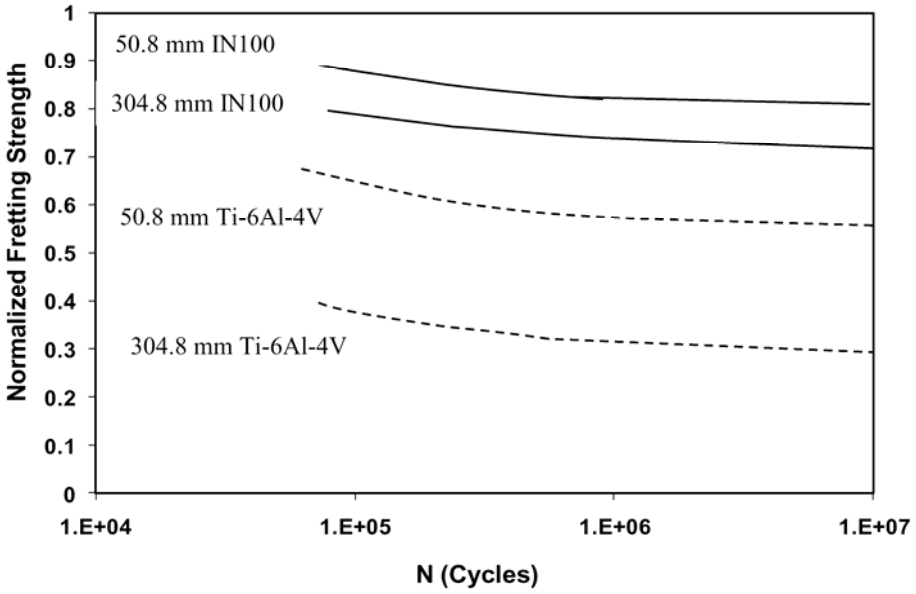

Figure 14. Normalized fretting fatigue strength for two contact geometries for IN100 and Ti-6Al-4V.

4.2. Fatigue parameter

Fretting fatigue life relationships, shown in Figure 12, are based on the applied stress to the specimen. Therefore, they do not account for the contact stress state, which is of the multi-axial nature and depends upon the contact geometry as discussed earlier (see Figure 11). Therefore, effects from the contact stress on the fretting fatigue should be considered. This can be done through the critical plane based fatigue parameters, which are commonly used in the multi-axial conventional fatigue studies. A previous study developed a critical plane-based parameter, modified shear stress range (MSSR), which has been shown to be effective in predicting fretting fatigue life from the plain fatigue data as well as the orientation and location of crack initiation in the titanium alloy, Ti-6Al-4V, when tested with various contact geometries [17]. This parameter was also utilized in the present study to analyze the fretting fatigue behaviour of IN100.

To compute the MSSR parameter, shear stress was calculated along all planes (i.e., from $-\pi/2$ to $\pi/2$ at an interval of 1°) at all points in the contact region. Then, shear stress range was calculated along all planes at all points in the contact region, i.e., $\Delta\tau = (\tau_{max} - \tau_{min})$, where τ_{max} and τ_{min} are the shear stresses corresponding to the maximum and minimum applied loads on the specimen during a fatigue cycle, respectively. From these, value of the maximum shear stress range, its location and the plane on which it is acting, i.e., critical plane, were determined. Since the mean stress or stress ratio also affects the fatigue behaviour, this effect on the critical plane was accounted for by a technique proposed by Walker [19]. This provided the effective maximum shear stress range on the critical plane, which is equal to:

$$\Delta\tau_{crit} = \tau_{max}(1 - R_\tau)^m, \tag{2}$$

where m is a fitting parameter to data at different stress ratios and R_τ is the stress ratio on the critical plane, i.e., $R_\tau = \tau_{min} / \tau_{max}$. The fitting parameter, m is assumed to be 0.45 in this study, which is the same as the one used in Ti-6Al-4V [17]. This was done due to unavailability of data at different stress ratios for IN100. Finally, the MSSR parameter was calculated by combining $\Delta\tau_{crit}$ and the normal stress on the critical plane for the maximum applied load on the specimen as:

$$\text{MSSR} = A(\Delta\tau_{crit})^B + C(\sigma_{max})^D, \tag{3}$$

where A, B, C & D are constants determined by curve fitting. These were 0.75, 0.5, 0.75, and 0.5, respectively, for Ti-6Al-4V [17]. This study used the same constants. Figure 15 shows the fretting fatigue from the two geometries as well as from the plain fatigue life data as a function of the MSSR parameter. This figure shows that MSSR parameter collapses the fatigue life data from two contact geometries together as well as those from the plain fatigue. Both fretting fatigue and plain fatigue life data lie on a single trend (as shown by the curve in the figure) with a mean error

of $\pm 0.1\%$ and a standard deviation of 1.5. It is worth mentioning here that, the curve fitting constants (A, B, C, D) appears to not dependent on the contact geometry as well as on two materials (IN100 and Ti-6Al-6V). But, the value of MSSR parameter at a given cycles to failure was different between these two materials such that, it was larger for IN100 than for Ti-6Al-4V. This suggests that MSSR versus cycle relationship is similar in shape for both materials. However, further studies are needed to ascertain this.

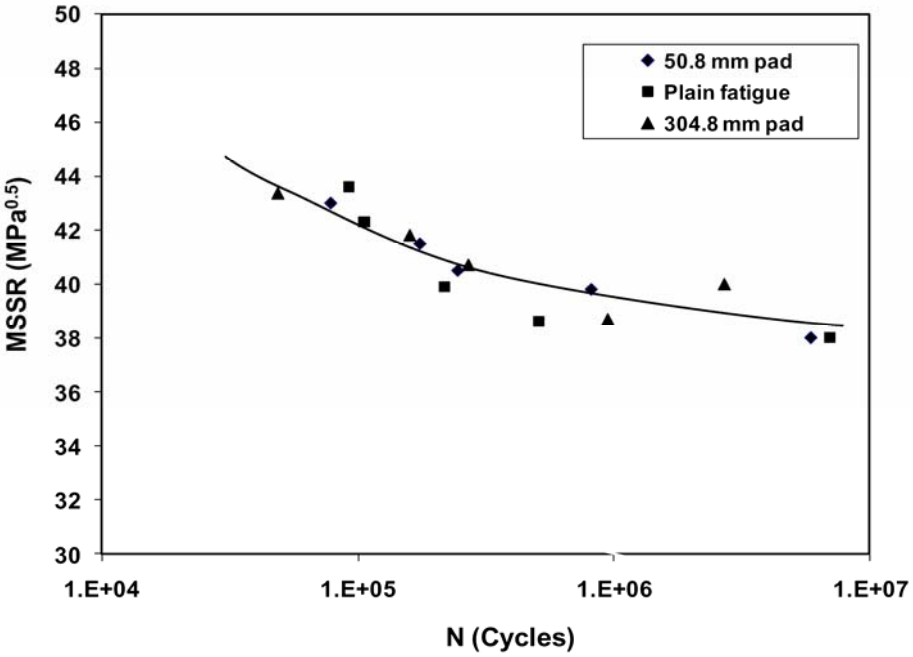

Figure 15. MSSR versus cycles to failure for two contact geometries and plain fatigue.

Further, the MSSR parameter was maximum at the contact surface near the trailing edge (x/a between 0.98 and 0.96). In other words, the MSSR parameter predicted the crack initiation location that was on the contact surface near the trailing edge (x/a between 0.98 and 0.96). This matched well with the experimental observation as mentioned earlier. In addition, the critical plane orientation was ±45° with variation of ±5°, i.e.,

MSSR also predicted crack initiation angle, which matched again well with the experimental measured orientation of crack initiation (Figure 9). As mentioned earlier, Figure 15 shows that the plain fatigue and fretting fatigue life versus MSSR relationships are in good agreement with each other. This means that the MSSR parameter can be used to predict the fretting fatigue crack initiation life from the plain fatigue data. Furthermore, MSSR parameter suggests that fretting fatigue behaviour of IN100 is affected by both shear and normal stresses on the critical plane. All these observations with IN100 are very similar to those with Ti-6Al-4V [17].

5. Conclusions

This study investigated the fretting fatigue behaviour of a nickel based alloy, IN100 at room temperature with cylinder-on-flat contact condition. Two cylindrical contact geometries were used by changing the fretting pad radius. Failure and damage mechanisms were investigated. Finite element method was also used to analyze the fretting fatigue behaviour by using a critical plane based fatigue parameter. The following conclusions can be drawn from the present study:

1. Fretting fatigue life at an applied stress was shorter than its plain fatigue counterpart.

2. Two contact geometries, one cylindrical and other one almost flat, showed similar trend in terms of fretting fatigue life at a given applied stress. However, almost flat contact geometry (i.e., larger cylindrical radius) had slightly shorter life at a given applied stress level.

3. Fretting crack initiation location was near the trailing edge at the contact surface, and crack initiation orientation angle at the contact surface was ±45° with a variation of ±10°.

4. A modified shear stress range parameter, involving both normal and shear stresses on the critical plane, correlated the fatigue life data from the two contact geometries as well as from the plain fatigue life data on a single trend. Further, it predicted fretting fatigue crack location and orientation, which were in agreement with the experimental counterparts.

5. The IN100 is relatively more fretting fatigue resistant in comparison to Ti-6Al-4V. Additionally, increase in cylindrical pad radius had relatively less detrimental effect on the fretting fatigue life/strength of IN100 in comparison to titanium alloy, Ti-6Al-4V.

References

[1] M. H. Attia and R. B. Waterhouse, Eds., Standardization of Fretting Fatigue Test Methods and Equipment, ASTM STP 1159, American Society for Testing and Materials, Philadelphia, 1992.

[2] M. H. Attia, Fretting Fatigue of Some Nickel-based Alloys in Steam Environment at 265ºC, Fretting Fatigue: Current Technology and Practices, ASTM STP 1367, D. W. Hoeppner, V. Chandrasekaran and C. B. Elliott, Eds., American Society for Testing and Materials, West Conshohocken, PA, (2000), 231-246.

[3] T. Hansson, M. Kamaraj, Y. Mutoh and B. Peterson, High Temperature Fretting Fatigue Behaviour in an XDTM γ- base TiAl, Fretting Fatigue: Current Technology and Practices, ASTM STP 1367, D. W. Hoeppner, V. Chandrasekaran and C. B. Elliott, Eds., American Society for Testing and Materials, West Conshohocken, PA, (2000), 65-79.

[4] D. A. Hills and D. Nowell, Mechanics of Fretting Fatigue, Kluwer Academic Publishers, Dordrecht, 1994.

[5] D. W. Hoeppner, V. Chandrasekaran and C. B. Elliott, Eds., Fretting Fatigue: Current Technologies and Practice, ASTM STP 1367, American Society for Testing and Materials, West Conshohocken, 2000.

[6] K. Iyer and S. Mall, Effects of cyclic frequency and contact pressure on fretting fatigue under variable-amplitude loading, Fatigue & Fracture of Engineering Materials and Structures 23 (2000), 335-346.

[7] S. E. Kinyon, D. W. Hoeppner and Y. Mutoh, Eds., Fretting Fatigue: Advances in the Basic Understanding and Applications, ASTM STP 1425, American Society for Testing and Materials, West Conshohocken, 2003.

[8] J. D. Kwon, Y. S. Chai, Y. T. Bae and S. J. Choi, A study on fretting behaviour in room temperature for Inconel alloy 690, International Journal of Modern Physics B 20 (2006), 4303-4308.

[9] H. Lee, O. Jin and S. Mall, Fretting fatigue behaviour of Ti-6Al-4V with dissimilar mating materials, International Journal of Fatigue 26 (2004), 393-402.

[10] H. Lee and S. Mall, Effect of dissimilar mating materials and contact force on fretting fatigue behaviour of Ti-6Al-4V, Tribology International 37 (2004), 35-44.

[11] C. D. Lykins, S. Mall and V. K. Jain, Combined experimental-numerical investigation of fretting fatigue crack initiation, International Journal of Fatigue 23 (2001), 703-711.

[12] C. D. Lykins, S. Mall and V. K. Jain, A shear stress-based parameter for fretting fatigue crack initiation, Fatigue & Fracture of Engineering Materials and Structures 24 (2001), 461-473.

[13] S. Mall, J. L. Ng and E. Madhi, Fretting fatigue behaviour of shot-peened Ti-6Al-4V and IN100, Journal of ASTM International 5 (2008).

[14] K. Miyoshi, B. A. Lerch, S. L. Draper and S. V. Raj, Evaluation of Ti-48Al-2Cr-2Nb under Fretting Fatigue Conditions, Fretting Fatigue: Advances in Basic Understanding and Applications, ASTM STP 1425, Y. Mutoh, S. E. Kinyon and D. W. Hoeppner, Eds., American Society for Testing and Materials, West Conshohocken, PA, (2003), 323-337.

[15] H. Murthy, D. B. Garcia, J. F. Matlik and T. Farris, Fretting fatigue of single crystal/polycrystalline nickel subjected to blade/disk contact loading, Acta Astronautica 57 (2005), 1-9.

[16] H. Murthy, G. Gao and T. Farris, Fretting fatigue of single crystal nickel at 600°C, Tribology International 39 (2006), 1227-1240.

[17] S. A. Namjoshi, S. Mall and V. K. Jain, Fretting fatigue crack initiation mechanism in Ti-6Al-4V, Fatigue & Fracture of Engineering Materials and Structures 25 (2002), 955-964.

[18] C. T. Tsai and S. Mall, Elasto-plastic finite element analysis of fretting stresses in pre-stressed strip in contact with cylindrical pad, Finite Elements in Analysis and Design 36 (2000), 171-187.

[19] K. Walker, The Effect of Stress Ratio during Crack Propagation and Fatigue for 2024-T3 and 7075-T6 Aluminum, Effects of Environment and Complex Load History on Fatigue Life, ASTM STP 462, American Society for Testing and Materials, Philadelphia, PA, (1970), 1-14.

[20] R. H. Wang, V. K. Jain and S. Mall, A non-uniform friction distribution model for partial slip fretting contact, Wear 262 (2007), 607-616.

■